Discovery of an inhibitor of insulin-like growth factor 1 receptor activation: Implications for cellular potency and selectivity over insulin receptor

Edgar R. Wood [a],*, Lisa Shewchuk [b], Anne Hassel [b], Jim Nichols [a], Anne T. Truesdale [a], Danielle Smith [a], H. Luke Carter [a], Kurt Weaver [a], George Barrett [a], Tony Leesnitzer [c], Emilio Alvarez [c], Ana Isabel Bardera [c], Amelia Alamillo [c], Juan Cantizani [c], Julio Martin [c], Gary K. Smith [c], David E. Jensen [a], Hongbo Xie [a], Robert Mook [d], Rakesh Kumar [e], Kevin Kuntz [d]

[a] Department of Biological Reagents and Assay Development, Research Triangle Park, GlaxoSmithKline, Inc., 5 Moore Drive, NC 27709, United States
[b] Department of Computational and Structural Chemistry, Research Triangle Park, GlaxoSmithKline, Inc., 5 Moore Drive, NC 27709, United States
[c] Department of Screening and Compound Profiling, Research Triangle Park, GlaxoSmithKline, Inc., 5 Moore Drive, NC 27709, United States
[d] Department of Oncology Chemistry, GlaxoSmithKline, Inc., 5 Moore Drive, Research Triangle Park, NC 27709, United States
[e] Department of Oncology Biology, 1250 South Collegeville Road, Collegeville, PA 19426, United States

ARTICLE INFO

ABSTRACT

Insulin-like growth factor 1 receptor (IGF-1R) is an attractive target for anti-cancer therapy due to its anti-apoptotic effect on tumor cells, but inhibition of insulin receptor (IR) may have undesired metabolic consequences. The primary sequences of the ATP substrate-binding sites of these receptors are identical and the crystal structures of the activated kinase domains are correspondingly similar. Thus, most small-molecule inhibitors described to date are equally potent against the activated kinase domains of IGF-1R and IR. In contrast, the non-phosphorylated kinase domains of these receptors have several structural features that may accommodate differences in binding affinity for kinase inhibitors. We used a cell-based assay measuring IGF-1R autophosphorylation as an inhibitor screen, and identified a potent purine derivative that is selective compared to IR. Surprisingly, the compound is a weak inhibitor of the activated IGF-1R tyrosine kinase domain. Biochemical and structural studies are presented that indicate the compound preferentially binds to the ATP site of non-phosphorylated IGF-1R compared to phosphorylated IGF-1R. The potential selectivity and potency advantages of this binding mode are discussed.

© 2009 Elsevier Inc. All rights reserved.

1. Introduction

The insulin-like growth factor 1 receptor (IGF-1R[1]) is a transmembrane receptor tyrosine kinase. The mature receptor has a heterotetrameric structure of two extracellular ligand-binding α-chains linked by disulfide bonds to two β-chains that span the membrane and contain the tyrosine kinase catalytic activity [1]. The unliganded receptor exists in a low activity, non-phosphorylated form. Binding of the ligands, insulin-like growth factors 1 or 2 (IGF-1 or IGF-2), elicits a conformational change that allows trans-phosphorylation of the β-chains. Three tyrosine residues in the kinase domain activation loop are phosphorylated resulting in structural rearrangement and a significant increase in kinase activity [2]. Activation of the kinase results in phosphorylation of intracellular substrates including insulin receptor substrates 1–4 (IRS1–4) and different Shc isoforms. These phosphorylation events trigger two key signal transduction cascades leading to AKT and extracellular-signal-regulated kinase (ERK) activation, which promote growth and survival of cells [3–5].
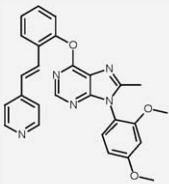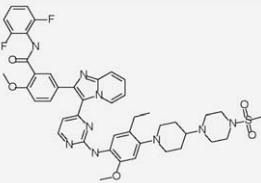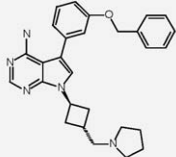
IGF-1R signaling plays a significant role in cancer. IGF-1R overexpression results in cellular transformation to a malignant phenotype and cells lacking IGF-1R are resistant to transformation by a variety of other oncogenes [3,5,6]. Furthermore, many human tumors overexpress IGF-1R and activation increases metastatic propensity [7]. For these and other reasons, IGF-1R has become an attractive target for anti-cancer therapy [8,9]. Inhibitors of kinase activity are one approach for targeting receptor tyrosine kinases [10,11]. For example, the epidermal growth factor receptor (EGFR)

---

* Corresponding author at: P.O. Box 13398, Research Triangle Park, NC 27709-13398, United States. Tel.: +1 919 483 3910; fax: +1 919 315 6720.
  E-mail address: erw39216@gsk.com (E.R. Wood).
[1] The abbreviations used are: IGF-1R, insulin-like growth factor 1 receptor; IR, insulin receptor; IRS, insulin receptor substrate; ERK, extracellular-signal-regulated kinase; EGFR, epidermal growth factor receptor; DMEM, Dulbecco's modified Eagles medium; ECL, electrochemiluminescence; GST, glutathione S-transferase; BSA, bovine serum albumin; FBS, fetal bovine serum; DTT, dithiothreitol; DMSO, dimethylsulfoxide; DELFIA, dissociation-enhanced lanthanide fluorescent immunoassay.

Table 1
Properties of IGF-1R inhibitors.

Compound	Cellular PY		Activated enzyme substrate PY	
	IGF-1R	IR	GST-IGF-1R$_{cat}$	GST-IR$_{cat}$
Compound 1	IC$_{50}$ (nM) 110 (50)	2994 (618)	IC$_{50}$ (nM) 3300 (2300)	4000 (700)
GSK4529	22	19	1.6	1.3
NVP-AEW541	90	2300	150	140

For compound 1, inhibition of ligand-stimulated receptor autophosphorylation was evaluated in NIH3T3 cells stably overexpressing either IGF-1R or IR (Cellular PY). Peptide substrate phosphorylation reactions were conducted using purified, fully activated GST-IGF-1R$_{cat}$ or GST-IR$_{cat}$. Data represents the average of at least three independent experiments. The standard deviation of the mean is shown in parentheses. Results for GSK4529 and NVP-AEW541 have been described previously [15,19].

and ErbB-2 inhibitor, lapatinib, has been approved for advanced breast cancer and selective EGFR inhibitors, gefitinib and erlotinib, are approved for the treatment of non-small cell lung cancer [12,13]. Several inhibitors of IGF-1R tyrosine kinase activity have been described that have activity in pre-clinical cancer models [14–17].

A challenge for the development of IGF-1R-targeted kinase inhibitors may be the catalytic domain similarity to the highly related insulin receptor (IR). Inhibition of IR would be expected to have significant effects on glucose homeostasis and chronic treatment may result in symptoms of diabetes [3]. The majority of kinase inhibitors described to date bind to the ATP site of the catalytic domain. For IGF-1R and IR, the amino acid sequences of the catalytic domains are 84% identical, and the ATP sites are 100% identical [18]. GSK4529 is a typical ATP-competitive IGF-1R inhibitor [19]. The compound is an equipotent inhibitor of purified IGF-1R and IR kinase domains. In cells, GSK4529 inhibits IGF-1R and IR autophosphorylation with similar potency that is reduced relative to the K_i for inhibition of the purified enzyme. This is expected for an ATP-competitive compound since the cellular ATP concentration is high (1–2 mM). BMS-554417 is a potent inhibitor of IGF-1R [16]. The compound inhibits the purified enzyme (IC$_{50}$ = 68 nM), IGF-stimulated receptor autophosphorylation in cell culture and tumor growth in mice. The compound is also an equipotent inhibitor of purified IR (IC$_{50}$ = 51 nM). Treatment with BMS-554417 was found to result in transient increases in insulin and glucose levels in mice. The dual inhibition of IGF-1R and IR and the physiological effects on glucose homeostasis reported for these compounds are consistent with the structural similarity and biological functions of the receptors. Another compound, NVP-AEW451, appears to have a different mode of inhibition [15]. This compound inhibits purified IGF-1R and IR with similar potency

(IC$_{50}$ = 150 and 140 nM respectively). However, in intact cells the compound is selective for IGF-1-stimulated IGF-1R autophosphorylation (IC$_{50}$ = 90 nM) compared to insulin-stimulated IR autophosphorylation (IC$_{50}$ = 2300 nM). Moreover, treatment with NVP-AEW451 at doses that blocked tumor growth did not result in an increase in insulin or glucose levels in mice. With NVP-AEW451, selectivity for IGF-1R over IR is observed in intact cells but not in assays measuring substrate phosphorylation catalyzed by the purified, activated catalytic domains.

We conducted a high-throughput screen of the GlaxoSmithKline compound collection for inhibitors of IGF-1R. Typically, receptor tyrosine kinase inhibitor screens are conducted using recombinantly expressed, purified, catalytic domains [20,21]. However, because of the challenges of IGF-1R selectivity, we developed a high-throughput assay that measures IGF-1-stimulated receptor autophosphorylation in intact cells. We identified compound 1 that potently inhibited receptor autophosphorylation (Table 1). Interestingly, compound 1 is a poor inhibitor of the purified, activated catalytic domain. Moreover, we also observe selectivity over insulin-stimulated IR autophosphorylation.

2. Materials and methods

2.1. Materials

Dimethylsulfoxide (DMSO), bovine serum albumin (BSA), Triton X-100, IGEPAL CA630, sodium deoxycholate, sodium orthovanadate, sodium fluoride, insulin, HEPES, MgCl$_2$, ATP, dithiothreitol (DTT), CHAPS, EDTA, MOPS, and sodium citrate were from Sigma–Aldrich (St. Louis, MO). Dulbecco's modified Eagle's medium (DMEM)/F-12, fetal bovine serum (FBS), and

geneticin were from Invitrogen (Carlsbad, CA). CellBind was from Corning (Lowell, MA). Protease inhibitor cocktail was from Thermo Fisher Scientific (Rockford, IL). IGF-1 was from R&D systems (Minneapolis, MN). Jeffamine M89 and perfluoropolyether were from Hampton Research (Aliso Viejo, CA).

2.2. Cell lines and culture conditions

NIH 3T3 cells that overexpress human IGF-1R (NIH-3T3/LISN) or IR (NIH-3T3-hIR) were obtained from Dr. Michael Kaleko [22]. Growth media was DMEM/F-12 with 10% fetal bovine serum (FBS) and 0.5 mg/ml geneticin. Cell stocks were produced using 10-stack cell factories with CellBind surface with proliferation to 85% confluence, and harvested with trypsin-EDTA. Cells were washed and resuspended in 90% FBS, 10% DMSO for storage in liquid nitrogen. Prior to use in the assay, cells were placed in a 37 °C water bath until nearly thawed, then slowly diluted 20-fold with phenol red-free DMEM (henceforth referred to as media buffer) plus 2 mg/ml BSA. After 15 min at room temperature, cells were pelleted by centrifugation, resuspended in media buffer, counted, and diluted to 5×10^5 cells/ml.

2.3. Cellular receptor autophosphorylation

The high-throughput screen for inhibitors of IGF-1R autophosphorylation in whole cells was conducted using an electrochemiluminescence (ECL)-based immunoassay format [23]. Ten μl of IGF-1R or IR overexpressing cell suspension, prepared as described above, were added to a 384-well avidin-coated MA6000 ECL assay plate from Meso Scale Discovery (Gathersburg, MD), containing 10 μl of test compound in media buffer. The cells were allowed to incubate with the compound for 2 h at room temperature prior to stimulation with IGF-1 or insulin (10 nM in 10 μl media buffer). After stimulation, the cells were incubated for 30 min at room temperature. The cells were lysed by adding 10 μl of lysis buffer consisting of 4× Read Buffer T (Meso Scale Discovery, Gathersburg, MD), 1.5% (w/v) Triton X-100, 1.5% (w/v) IGEPAL CA630, sodium deoxycholate (4 mg/ml), 4 mM sodium orthovanadate, 40 mM sodium fluoride, and 10 mM protease inhibitor cocktail. Antibodies for receptor capture and phosphotyrosine antibody for product detection were added directly to the lysis buffer prior to addition to the plate to a final concentration of 800 ng/ml of each. For IGF-1R and IR assays, the capture antibodies were MS641-B and MS631-B, respectively (Thermo Fisher Scientific, Freemont, CA). Phosphotyrosine was quantified using PY20 anti-phosphotyrosine antibody (Meso Scale Discovery, Gathersburg, MD). Plates were incubated in a dark, sealed humidity chamber at 4 °C to prevent evaporation. After 2 days, plates were brought to room temperature (usually 2 h) before reading using the Sector 6000 ECL detector (Meso Scale Discovery, Gathersburg, MD).

For immunoblot experiments, logarithmically growing NIH-3T3/LISN or NIH-3T3-hIR cells were serum starved for 2 h in the presence of compound and stimulated with IGF-1 or insulin as described above. After 30 min, cells were lysed and evaluated by immunoblot. One sample was analyzed for total receptor and the parallel sample was analyzed for phosphotyrosine containing receptor. Total IGF-1R was detected using antibody sc-713, and total IR was detected using antibody sc-711 from Santa Cruz Biotechnology (Santa Cruz, CA). Phosphotyrosine containing proteins were detected using mouse monoclonal antibody 05-321X (Millipore-Upstate, Billerica, MA).

2.4. IGF-1 and insulin signaling in human adipocytes

Primary human pre-adipocytes were obtained from ZenBio (RTP, NC) and were cultured and differentiated essentially as described by the supplier. Following differentiation, cells were serum starved overnight in DMEM/F-12, 1% BSA. The adipocytes were treated with compound for 1 h and stimulated for 5 min with IGF-1 (5 nM) or insulin (5 nM). Cells were lysed and AKT Ser473 phosphorylation was assessed using the ECL-immunoassay phospho-AKT kit. (Mesoscale Discovery, Gathersburg, MD).

2.5. Protein expression and purification

Kinase assays were performed using the intracellular domains of IGF-1R (amino acids 957–1367, Genbank NM000875.3) or IR (amino acids 977–1382, Genbank NM000208.2) fused to glutathione-S-transferase (GST). These constructs are referred to as GST-IGF-1R$_{cat}$ and GST-IR$_{cat}$. Protein structural studies were conducted using a construct consisting of amino acids MKKGHHHHHHG fused to amino acids 1017–1322 of IR, referred to as 6His-IR. The constructs were expressed using baculovirus and purified as described [24,25].

2.6. Activation and substrate phosphorylation assays

GST-IGF-1R$_{cat}$ and GST-IR$_{cat}$ were activated by autophosphorylation prior to conducting substrate phosphorylation reactions. The proteins were incubated at a concentration of 2.7 μM in 50 mM HEPES, pH 7.5, 10 mM MgCl$_2$, 0.1 mg/ml BSA and 2 mM ATP for 4 min at room temperature. The reaction was terminated by the addition of EDTA to 100 mM. The phosphorylation states of the proteins were analyzed by intact protein mass-spectrometry. Both proteins were not phosphorylated prior to activation. For GST-IGF-1R$_{cat}$ the procedure generated protein of the predicted molecular weight plus 6 additional phosphates. For GST-IR$_{cat}$ the activation procedure generated protein of the predicted molecular weight plus 7 additional phosphates. These results are consistent with those previously reported [24].

Substrate phosphorylation reactions were conducted using a homogeneous time-resolved fluorescence assay [26]. Assays were conducted in 10 μl of 50 mM HEPES pH 7.5, 3 mM DTT, 0.1 mg/ml BSA, 1 mM CHAPS, 10 mM MgCl$_2$, 500 nM IGF-1R peptide, biotin-aminohexyl-AEEEEYMMMMAKKKK-NH2 [27], and 10 μM ATP. Reactions were initiated by adding activated GST-IGF-1R$_{cat}$ or GST-IR$_{cat}$ to a final concentration of 0.5 nM and the plates were incubated for 1 h at room temperature. The reactions were terminated by adding 5 μl per well 100 mM EDTA followed by adding 5 μl product detection mix: 100 mM HEPES, pH 7.5, 0.1 mg/ml BSA, 1 mM CHAPS, 28 nM streptavidin-APC (PerkinElmer, Waltham, MA), 4 nM LANCE europium-labeled anti-phosphotyrosine antibody (PerkinElmer, Waltham, MA). The terminated reactions were allowed to equilibrate at room temperature for 30 min prior to data collection in a Viewlux imager (PerkinElmer, Waltham, MA).

2.7. Purified catalytic domain autophosphorylation

Autophosphorylation reactions were performed in a final reaction volume of 20 μl. The reaction contained 1 nM non-activated GST-IGF-1R$_{cat}$ or 0.5 nM non-activated GST-IR$_{cat}$, 100 mM HEPES, pH 7.5, 1 mM CHAPS, 2 mM DTT, 0.2 mg/ml BSA, 20 mM MgCl$_2$, 100 μM ATP. The reaction was incubated for 1 h at room temperature and then stopped by the addition of 40 μl/well 100 mM EDTA, 4% BSA. Receptor phosphorylation was detected using a dissociation-enhanced lanthanide fluorescent immunoassay (DELFIA) [28]. Total receptor was captured using anti-GST antibody (Millipore-Chemicon, Billerica, MA), and phosphotyrosine was quantified using europium-labeled N1 anti-phosphotyrosine (PerkinElmer, Waltham, MA). The ATP K_m for autophosphorylation was determined from time-course

experiments run in duplicate. For each ATP concentration, initial rates were determined from the linear portion of a 60 min time course sampled at 5 min intervals. V_{max} and K_m values were estimated from these experiments by fitting the data to Eq. (A):

$$v = \frac{V_{max} \times [\text{ATP}]}{K_m + [\text{ATP}]} \qquad (A)$$

2.8. Compound handling and data analysis for inhibitor testing

All compounds were dissolved from solid stocks in DMSO. For IC_{50} determination primary data was normalized and expressed as % inhibition:

$$\%I = 100 \times \frac{(U\text{-}C_1)}{(C_2\text{-}C_1)}$$

where U is the assay result in the presence of compound, C_1 is the average of the high signal in the absence of compound and C_2 is the average of the low signal (obtained using an excess of a known inhibitor or other appropriate negative control, such as EDTA). The normalized data was fit to a four parameter logistic function:

$$y = \frac{(B \times x^n)}{(K^n + x^n)} + A \qquad (B)$$

where $y = \%I$, B = minimum asymptote (typically no inhibition), x = compound concentration, $K = IC_{50}$, A = maximum asymptote (typically 100% inhibition), and n represents the slope factor of the inhibition curve (typically close to 1). Eq. (B) was also used to analyze IGF-1 and insulin stimulation of AKT phosphorylation in human adipocytes. In this case K = concentration of ligand that generated 50% of the maximum effect (EC_{50}).

2.9. Crystallization and structure solution

6-His-IR (10 mg/ml) was incubated with a 3-fold molar excess of compound 5 for 1 h prior to crystallization. Crystals were grown by the hanging drop vapor diffusion method at 22 °C from 0.1 M MOPS pH 7.0, 1.2 M NaCitrate and 1% Jeffamine M89. Crystals were flash frozen in liquid nitrogen prior to data collection using perflluorpolyether as a cryoprotectant. Data was collected at Beamline LS-CAT 21ID-D at Argonne National Laboratory's Advanced Photon Source. The data was processed with HKL2000 [29] and the structure was solved by molecular replacement using CCP4 Suite 6.0.2 from CCP4 group in the Computational Science and Engineering Department, Daresbury Laboratory (Daresbury, Warrington, Cheshire, UK).

3. Results

3.1. Cell-based screening for inhibitors of IGF-1R autophosphorylation

We conducted a high-throughput screen of all compounds ($\sim 2 \times 10^6$) in the GlaxoSmithKline collection using a whole-cell assay that measured IGF-1-stimulated IGF-1R autophosphorylation. Active compounds were counter-screened in similar fashion for inhibition of insulin-stimulated IR autophosphorylation. Compounds of interest were further evaluated for their ability to inhibit the tyrosine kinase activity of the purified intracellular domains expressed as GST-fusion proteins. These GST-fusion proteins, GST-IGF-1R_cat and GST-IR_cat, were activated by autophosphorylation following the methods described by Baer et al. [24].

We identified compound 1 that inhibits IGF-1R autophosphorylation in cells while not affecting total receptor levels (Fig. 1). The IC_{50} for inhibition of cellular IGF-1R autophosphorylation was 110 nM (Table 1). Interestingly, the compound
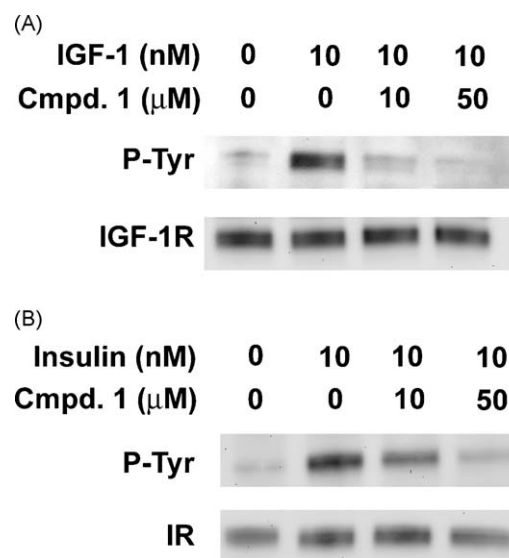
Fig. 1. Inhibition of IGF-1R and IR autophosphorylation. (A) Logarithmically growing NIH-3T3 cells stably overexpressing IGF-1R (NIH-3T3/LISN) were incubated with the indicated concentration of compound 1 in serum-free DMEM for 2 h. The cells were stimulated with IGF-1 as shown. After 30 min, cells were lysed and total IGF-1R or tyrosine phosphorylated receptor (P-Tyr) were detected by immunoblot. (B) Same as in A, except that IR overexpressing cells (NIH-3T3-hIR) were used and stimulated with insulin as shown.

was not a very potent inhibitor of substrate phosphorylation catalyzed by activated GST-IGF-1R_cat (IC_{50} = 3300 nM). Most kinase inhibitors are competitive with ATP. Therefore, the observed IC_{50} is related to the K_i of the compound, the K_m for ATP and the concentration of ATP as described in Eq. (C) [30].

$$IC_{50} = K_i \times \left(1 + \frac{[\text{ATP}]}{K_m}\right) \qquad (C)$$

We determined the ATP K_m for fully activated GST-IGF-1R_cat and found it to be 35 μM (data not shown), which is similar to values previously reported [2,31]. The GST-IGF-1R_cat substrate phosphorylation reaction was conducted using 10 μM ATP so the estimated K_i for GST-IGF1Rcat from Eq. (C) is 2500 nM. Cellular ATP concentrations are typically 1 mM or greater, so we would expect an approximately 30-fold increase in the cellular IC_{50} relative to the K_i. With compound 1, the cellular IC_{50} was 23-fold lower than the GST-IGF-1R_cat K_i. This unusual relationship between the K_i and cellular IC_{50} suggested that compound 1 functions through a mechanism other than typical ATP-competitive inhibition of substrate phosphorylation.

3.2. Mechanism of action of compound 1

Compound 1 was evaluated in a panel of 31 in vitro kinase assays (Table 2). Activated GST-IGF-1R_cat and GST-IR_cat were weakly inhibited (IC_{50} = 3300 and 4000 nM respectively). Of the other 29 kinases tested, only focal adhesion kinase (FAK) was inhibited (IC_{50} = 3600 nM). Based upon these results, it seems unlikely that inhibition of other cellular kinases is contributing to the observed cellular inhibition of IGF-1R tyrosine phosphorylation.

We evaluated the effect of ATP concentration on the apparent potency of inhibition of fully activated GST-IGF-1R_cat (Fig. 2). The IC_{50} increased as a function of increasing ATP concentration, consistent with the relationship described in Eq. (C). A fit of the results to this equation resulted in estimates of K_i of 1.1 μM and K_m for ATP of 32 μM. This suggests that the compound inhibits GST-IGF-1R_cat through an ATP-competitive mechanism.

Table 2
Kinase selectivity data.

Target name	Assay format	Compound 1		Compound 5	
		n	IC$_{50}$ (nM)	n	IC$_{50}$ (nM)
IGF-1R	HTRF	4	3,300 (2,300)	2	260 (60)
FAK	HTRF	3	3,700 (1,000)		n.d.
INSR	HTRF	3	4,000 (700)	2	820 (110)
ACTRIIB	Ligand binding	2	>10,000	1	>10,000
AKT1	SPA	4	>10,000	2	>10,000
AKT2	SPA	4	>10,000	2	>10,000
ALK	HTRF	3	>10,000	1	>10,000
ALK5	Ligand binding	4	>10,000	2	>10,000
ASK1	IMAP	3	>10,000	1	>10,000
AURORA A	IMAP	3	>10,000	2	8,300 (2,300)
CAMKK1	IMAP	1	>10,000	1	>10,000
CAMKK2	IMAP	2	>10,000		n.d.
COT1	IMAP	1	>10,000	1	>10,000
DDR2	HTRF	1	>10,000		n.d.
EGFR	HTRF	2	>10,000	2	>10,000
ERBB4	HTRF	2	>10,000		n.d.
GSK3b	Ligand binding	3	>10,000	1	>10,000
IKK2	HTRF	3	>10,000	1	>10,000
ITK	HTRF	2	>10,000	1	>10,000
JNK1	HTRF	4	>10,000	2	7,080 (4,000)
JNK2	HTRF	3	>10,000	1	>10,000
JNK3	Ligand binding	3	>10,000	1	>10,000
LCK	IMAP	3	>10,000	1	>10,000
P70S6K	IMAP	4	>10,000	1	>10,000
PAK1	IMAP	4	>10,000	2	>10,000
PDK1	SPA	4	>10,000	2	>10,000
ROCK1	IMAP	4	>10,000	2	>10,000
SYK	HTRF	3	>10,000	1	>10,000
VEGFR2	HTRF	1	>10,000	1	4,645

The IC$_{50}$ for the listed kinase was determined using the indicated assay format. Proteins were expressed in *Escherichia coli* or baculovirus-infected insect cells and purified by metal-chelate or glutathione affinity chromatography. Peptide substrate phosphorylation was measured using HTRF and SPA-based detection systems [20] or IMAP-based detection [46]. ATP-binding site ligand-displacement assays (ligand binding) were conducted essentially as described [47]. The average value of n experimental determinations is shown. The standard deviation of the mean is shown in parentheses. n.d., Not determined.

Compound 1 may bind differently to different phosphorylation states of IGF-1R. To test this, we established an assay using purified non-activated GST-IGF-1R$_{cat}$ that measures autophosphorylation upon incubation with ATP. We evaluated the reaction as a function of receptor concentration and time in order to select conditions where changes in the level of receptor phosphotyrosine were linear with respect to time and enzyme. These conditions were satisfied using 1 nM GST-IGF-1R$_{cat}$, 100 μM ATP, and an incubation time of 1 h (Fig. 3A). Using this assay, we found that compound 1 inhibited GST-IGF-1R$_{cat}$ autophosphorylation with an IC$_{50}$ of 260 nM (Table 3). This represents a 13-fold increase in potency over inhibition of activated GST-IGF-1R$_{cat}$ substrate phosphorylation and may explain the cellular potency of the compound (Fig. 3C). We determined the K_m for ATP for GST-IGF-1R$_{cat}$ autophosphorylation to be 1050 μM (Fig. 3B) which is very similar to the value reported by others [2,31]. The estimated K_i for autophosphorylation is therefore 283 nM. The high ATP K_m value for autophosphorylation may explain why there is little difference between the cellular IC$_{50}$ and the K_i for GST-IGF-1R$_{cat}$ autophosphorylation.

NVP-AEW541 is similar to compound 1 since it was shown to be selective for autophosphoryaltion in cells, but not in assays with the purified enzyme [15]. We evaluated inhibition of GST-IGF-1R$_{cat}$ by NVP-AEW541 and found that it was less potent for inhibition of autophosphorylation (IC$_{50}$ = 90 nM) compared to inhibition of activated GST-IGF-1R$_{cat}$ substrate phosphorylation (IC$_{50}$ = 30 nM).
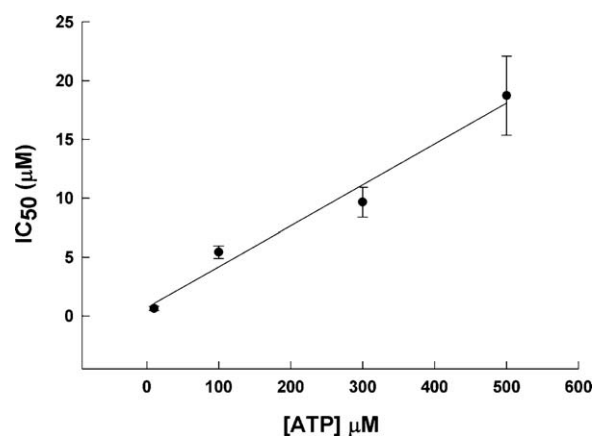
Fig. 2. The effect of ATP concentration on inhibition of GST-IGF-1R$_{cat}$ by compound 1. Substrate phosphorylation reactions catalyzed by activated GST-IGF-1R$_{cat}$ were conducted using the indicated concentration of ATP. The mean IC$_{50}$ of compound 1 determined from three independent experiments is plotted as a function of ATP concentration. Error bars represent the standard deviation of the mean. The solid line represents the least squares fit of these results to the competitive mechanism described in Eq. (C).

Our results for inhibition of activated GST-IGF-1R$_{cat}$ by NVP-AEW541 were somewhat lower than that reported (IC$_{50}$ = 150 nM) [15]. There were several differences in the two assay formats including peptide substrate sequence and concentration that may contribute to the observed IC$_{50}$ differences.

3.3. Optimization of IGF-1R activation inhibitors

We synthesized variants of compound 1 and measured inhibition of cellular autophosphorylation for IGF-1R and IR. We also measured inhibition of autophosphorylation of the purified GST-IGF-1R$_{cat}$ and GST-IR$_{cat}$ (Table 3). The basic template is defined by a core purine ring with 6-oxybenzyl-4-ethenylpyridine and 9-benzyl groups. The 2,4-dimethyl 9-benzyl ring substitution (compound 2) was similar to the 2,4-dimethoxy substitution of compound 1. The 4-methyl substitution of the 9-benzyl ring improved potency (compound 4), whereas the 2-methyl substitution reduced potency. A similar structure–activity relationship was observed for comparable Cl substitutions (data not shown). Loss of the 8-methyl group from the purine ring improved potency 2-fold (compound 5). Para-substitutions of the 6-oxybenzyl ring (compounds 6 and 7) negatively affected potency with some reduction in selectivity. Overall, the potency and selectivity observed in cells was reflected in the GST-IGF-1R$_{cat}$ and GST-IR$_{cat}$ autophosphorylation assays. Compound 5 provides the greatest cellular potency and selectivity of compounds in this series, and was selected for further studies.
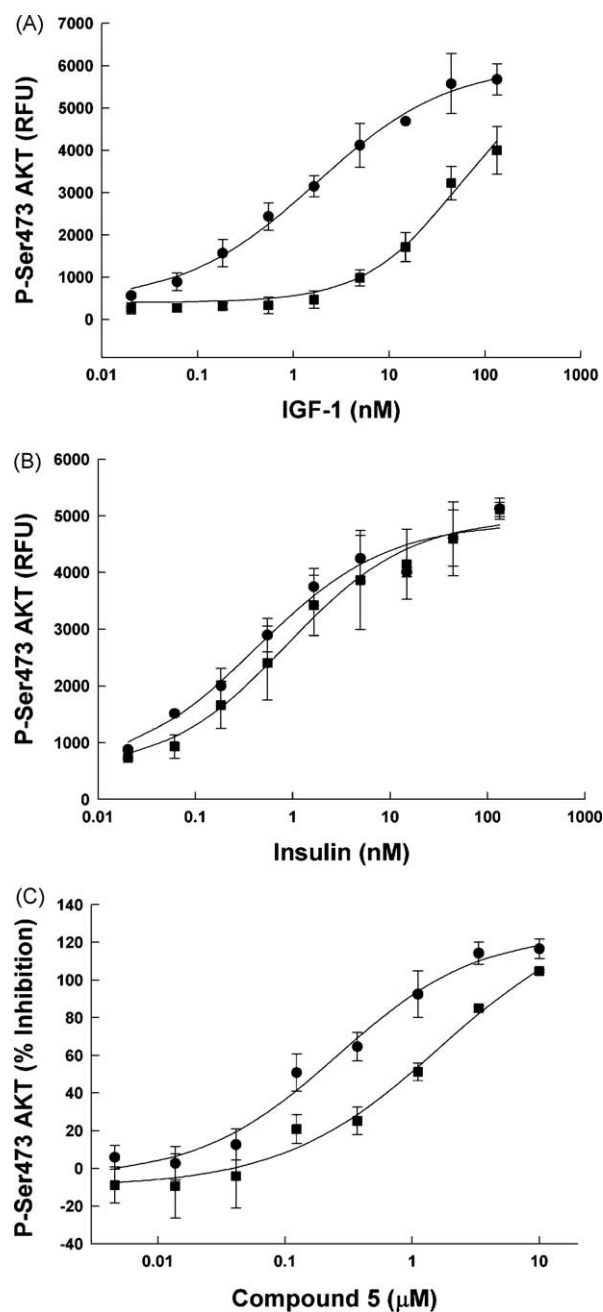
3.4. Inhibition of IGF-1 and Insulin signaling in primary human adipocytes

We evaluated primary human adipocytes to confirm the physiological relevance of the IGF-1R and IR inhibition. The effect of IGF-1 or insulin concentration on the level of phosphorylated AKT was determined. The EC$_{50}$ of insulin activation was 0.5 ± 0.3 nM (Fig. 4A). The EC$_{50}$ of IGF-1 activation was 1.7 ± 0.4 nM (Fig. 4B). These EC$_{50}$s are within the expected physiologically relevant range, but it is known that IGF-1 can activate the insulin receptor at higher concentrations. αIR3 is a neutralizing antibody that is selective for IGF-1R over IR [32]. αIR3 addition resulted in a significant increase in the EC$_{50}$ for IGF-1 stimulated AKT phosphorylation, but did not affect the EC$_{50}$ for insulin (Fig. 4A and B). Based upon these results, IGF-1 and
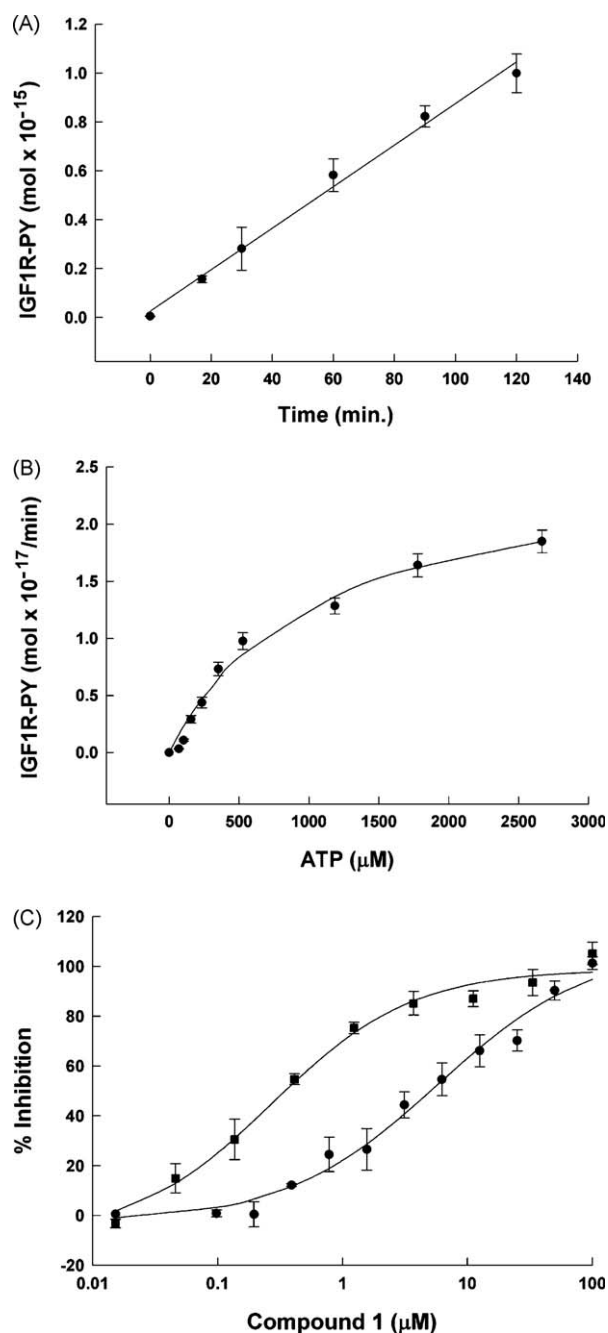
Fig. 3. Autophosphorylation of purified GST-IGF-1R$_{cat}$. Autophosphorylation beginning with non-phosphorylated GST-IGF-1R$_{cat}$ was analyzed using the DELFIA-based method. (A) Timecourse of autophosphorylation at 100 μM ATP. The solid line represents a linear fit of the results. (B) ATP substrate kinetic parameters. The initial rate of autophosphorylation was determined from timecourse studies and is plotted as a function of ATP concentration. The solid line represents the least squares fit of these results to Eq. (A). (C) Inhibition of GST-IGF-1R$_{cat}$ activity as a function of compound 1 concentration. (●) Substrate phosphorylation catalyzed by fully phosphorylated GST-IGF-1R$_{cat}$. (■) Autophosphorylation catalyzed by non-phosphorylated GST-IGF-1R$_{cat}$. The solid lines represent the least squares fit of the results to Eq. (B). In all panels, data represents the mean of three determinations and error bars represent the standard deviation of the mean.

Fig. 4. Compound 5 inhibition of IGF-1R or IR in human adipocytes. Differentiated human adipocytes were obtained as described under experimental procedures, and the amount of phosphorylated AKT (Ser473) was determined. (A) (●) Dose response of IGF-1. (■) Dose response of IGF-1 in the presence of 250 ng/ml αIR3 antibody. (B) (●) Dose response of insulin. (■) Dose response of insulin in the presence of 250 ng/ml αIR3 antibody. (C) AKT phosphorylation was measured in the presence of the indicated concentration of compound 5. (●) Stimulation with IGF-1 (5 nM). (■) Stimulation with insulin (5 nM). In all panels, data represents the mean of three determinations and error bars represent the standard deviation of the mean. The solid lines represent the least squares fit of the results to Eq. (B).
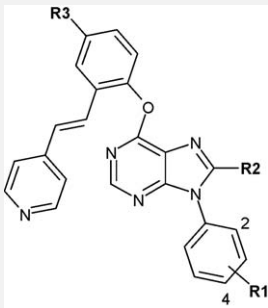
the adipocyte system. Compound 1 inhibited AKT phosphorylation with IC$_{50}$ values of 2200 ± 600 nM (IGF-1 stimulated) and 8500 ± 1700 nM (insulin stimulated).

3.5. Structure of compound 5 bound to the insulin receptor

The co-crystal structure of compound 5 complexed with the non-phosphorylated kinase domain of insulin receptor was solved to an R$_{factor}$/R$_{free}$ of 19.8/23.0% at 2.0 Å resolution. Additional

insulin signal exclusively through their respective receptors at or below 10 nM ligand. We evaluated the effect of compound 5 on IGF-1 and insulin stimulated AKT phosphorylation using 5 nM ligand (Fig. 4C). Compound 5 inhibited IGF-stimulated AKT phosphorylation with an IC$_{50}$ of 300 ± 140 nM, and insulin stimulated AKT phosphorylation with an IC$_{50}$ of 1500 ± 460 nM. Compound 1 was also characterized in

Table 3
Structure–activity relationships of IGF-1R activation inhibitors.

Compound	R1	R2	R3	Cellular-PY		GST$_{cat}$ Auto-PY	
				IGF-1R	IR	IGF-1R	IR
				IC$_{50}$ (nM)		IC$_{50}$ (nM)	
1	2,4-diOMe	Me	H	110 (50)	2994 (618)	257 (94)	926 (190)
2	2,4-diMe	Me	H	240 (47)	3547 (235)	92 (25)	225 (109)
3	2-Me	Me	H	600 (500)	>10^4	4700 (90)	>10^4
4	4-Me	Me	H	35 (30)	2528 (1354)	46 (10)	123 (40)
5	2,4-diMe	H	H	42 (21)	2764 (1509)	42 (10)	126 (45)
6	2,4-diMe	Me	Me	151 (24)	1384 (709)	282 (60)	534 (64)
7	2,4-diMe	Me	tBu	812 (201)	5601 (1215)	741 (140)	1859 (164)

Ligand-stimulated receptor autophosphorylation in cells (cellular PY), and purified enzyme autophosphorylation (GST$_{cat}$ Auto-PY) was determined for IGF-1R and IR as indicated. Data represents the average of at least 3 independent experiments. The standard deviation of the mean is shown in parentheses.

details of the refinement can be found in Table 4. Overall, the protein has an inactive conformation. The C helix is shifted relative to its position in the phosphorylated IR-ATP-peptide substrate complex [33], and the conserved Glu-Lys salt bridge is broken. Phe-1151 of the activation loop DFG motif is in the DFG-out position, and part of the activation loop is disordered.
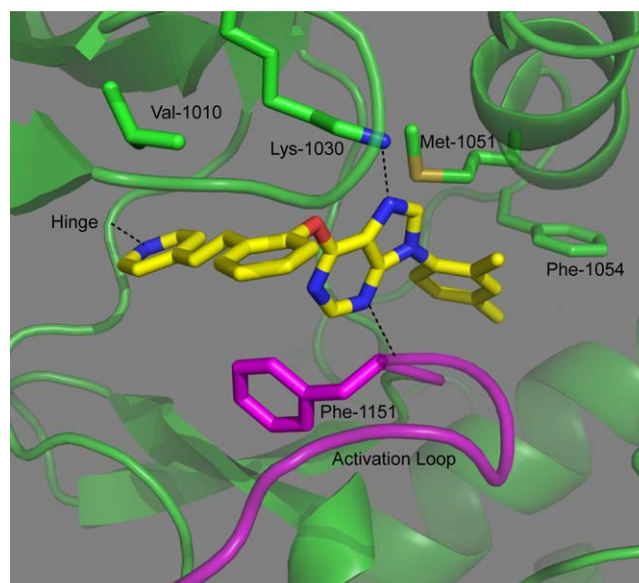
Compound 5 binds in the ATP-binding site extending deep into the back pocket (Fig. 5). The inhibitor pyridine makes a hydrogen bond to the backbone NH of Met-1079. Two additional hydrogen bonds are formed between the purine ring and the side chain of Lys-1030 and backbone NH of Asp-1150. The inhibitor 6-oxybenzyl ring is roughly located in the same position as the α phosphate of ATP and sandwiched between the side chains of Phe-1151 and Val-1010. The 9-dimethylbenzyl ring sits deep in a back pocket formed by the side chains of Val1-050, Met-1051, Phe-1054, Leu-1123 and Phe-1128.

Table 4
X-ray data collection and refinement statistics.

Space group	$P2_12_12$
Cell	a = 122, b = 117, c = 55, $\alpha = \beta = \chi = 90$
Data collection	
Resolution (Å)	122.0–2.0
Observations	338,815
Unique reflections	50,915
Completeness (%)	97.4
Completeness (%, high res)	83.8
I/sigma (all)	17.8
I/sigma (high res)	2.8
R_{sym} (%)	11.1
Refinement	
R_{factor} (%)	19.8
R_{free} (%)	23
RMS deviations	
Bond lengths (Å)	0.007
Bond angles (°)	1.015
Average B-factors (Å^2)	
All atoms	24.2

In the apo-non-phosphorylated crystal structure of IR, Phe-1151 of the activation loop DFG motif moves into the adenine binding pocket, partially blocking the ATP-binding site. In addition, the C helix is shifted upward such that the conserved Glu-Lys salt bridge is broken [34]. In the compound 5 cocrystal structure, residues 1149–1156 of the activation loop adopt a different conformation allowing Phe-1151 to shift ~4 Å and accommodate inhibitor binding (Fig. 6). A small shift in the relative orientation of the N and C-terminal lobes was also observed, leading to the ATP-binding cleft in the compound 5 complex to be more open than in the inactive apo-structure. In the active phosphorylated IR-ATP-


Fig. 5. Compound 5 interactions in the ATP-binding site of non-phosphorylated IR. The figure was derived from the crystal structure of compound 5 complexed with non-phosphorylated IR. The inhibitor is shown as a yellow stick figure. The protein is represented as a green cartoon with the activation loop highlighted in magenta. The figure was created with PYMOL (X).
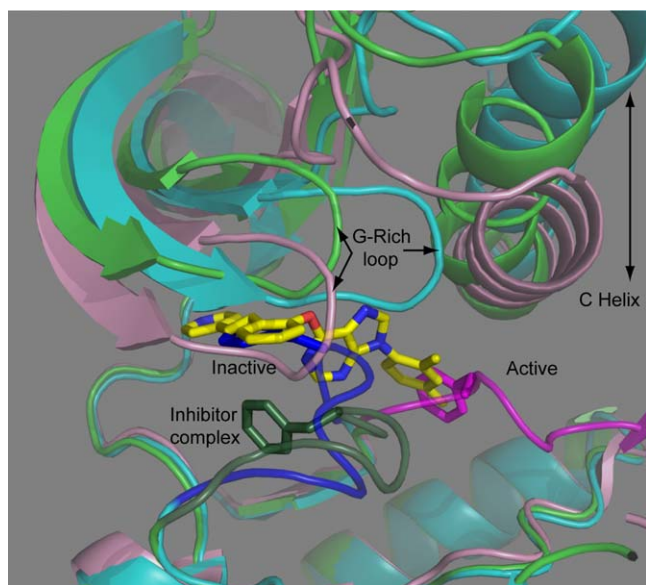
Fig. 6. Overlay of IR in its active, inactive and compound 5 bound conformations. The proteins were overlaid based on the C-alpha positions of all residues in the C-terminal domain. Active IR (PDB 1IR3) is shown in pink with a magenta activation loop. Inactive IR (PDB 1IRK) is shown in cyan and blue while the inhibitor structure is in light and dark green. Differences in the position of the C helix, G-rich loop and Phe-1151 are highlighted.
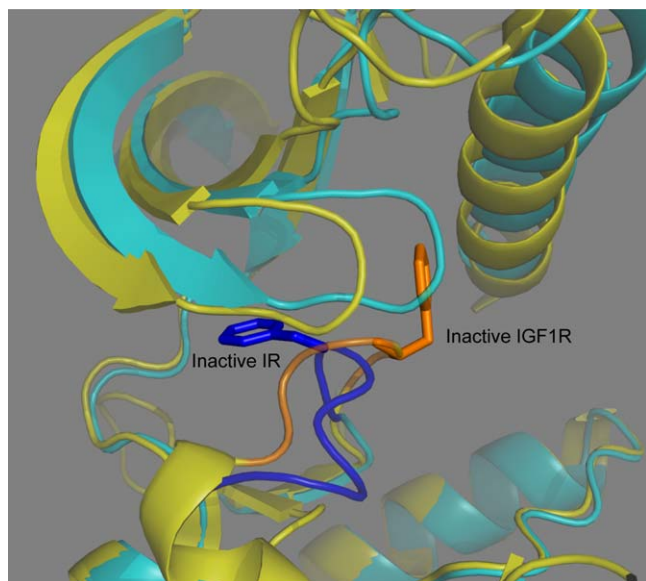
Fig. 7. Overlay of the inactive apo structures of IR and IGF-1R. The protein/activation loop of IR and IGF-1R are shown in cyan/blue and yellow/orange respectively. The positions of Phe-1151 (IR) and corresponding Phe-1124 (IGF-1R) are highlighted.

peptide complex, Phe-1151 points into the interior of the protein and the C helix is shifted down towards the C-terminal domain of the kinase (Fig. 6). In this conformation, there would be no room in the back of the ATP-binding pocket to accommodate the 9-dimethylbenzyl group of the inhibitor.

Comparison of the apo-non-phosphorylated crystal structures of IR [34] and IGF-1R [35] kinase domains reveals a number of structural differences. While the C helix is displaced in both structures relative to the active phosphorylated IR-ATP-peptide crystal structure [33], significant differences were observed in the activation loop conformation (Fig. 7). As described above, Phe-1151 of the activation loop blocks the ATP-binding site in the

inactive IR structure. In the inactive IGF-1R structure the corresponding residue, Phe-1124, points towards the back of the ATP site and its side chain is wedged between the side chains of the conserved Lys and Glu that form a salt bridge in the active conformation of the kinase. These differences in the inactive conformations may help explain the selectivity over IR we observe with the compounds in this series.

4. Discussion

Small-molecule kinase inhibitors typically function by binding to the ATP substrate site. Therefore, obtaining selectivity can be a challenge, especially between closely related proteins like IGF-1R and IR. In addition, the high ATP concentration may significantly reduce the cellular IC_{50} relative to the K_i of kinase inhibition. Compound 1 is unusual because the cellular IC_{50} (110 nM) is lower than the predicted K_i (2500 nM). The compound is also selective for inhibition of IGF-1R over IR in assays of cellular autophosphorylation. Because of these unusual properties, we hypothesized that compound 1 functioned through a mechanism other than binding to the ATP substrate site. Substrate competition studies, however, indicated that the compound inhibited GST-IGF-1R$_{cat}$ in an ATP-competitive fashion. In cells, ligand binding stimulates autophosphorylation that leads to activation of the kinase domain. Compound 1 was more than 10-fold more potent for inhibition of purified GST-IGF-1R$_{cat}$ autophosphorylation compared to inhibition of the fully phosphorylated protein. This suggests that the cellular potency of compound 1 results primarily from binding to the non-phosphorylated receptor.

We used knowledge of this binding mode to optimize the potency of compounds in this series. We found that 4-Me substitution of the 9-benzyl ring (compound 4) provided a significant increase in potency, and the unsubstituted purine ring (compound 5) also improved potency. Two trends in the data are noticeable: inhibition of cellular autophosphorylation was tightly correlated with inhibition of GST-IGF-1R$_{cat}$ autophosphorylation, and selectivity for inhibition of autophosphorylation between IGF-1R and IR was observed in cells and with purified GST-catalytic domains. The correlation of inhibition of cellular and GST-catalytic domain autophosphorylation within this compound series provides further support that binding to the non-phosphorylated form is responsible for the observed activity of these molecules. Munshi et al. proposed that selective inhibition of IGF-1R would be more feasible targeting the non-phosphorylated form of the receptor based upon crystal structure comparisons [36]. Our results support this prediction.

The IGF-1R and IR cellular autophosphorylation assays were conducted using over-expressing fibroblast cell lines. The number of receptors expressed by these cells ($\sim 1 \times 10^6$ receptors per cell) far exceeds the number expressed in normal tissue and primary cells [22]. The high receptor level might affect the apparent potency and selectivity, so we evaluated compound inhibition in primary human cells including lung fibroblasts, umbilical vein epithelial cells and differentiated adipocytes . Unfortunately, we could not accurately measure autophosphorylation of IGF-1R and IR in these cell types due to the low receptor number, but we could accurately measure IGF-1 and insulin stimulated AKT phosphorylation in lung fibroblasts and adipocytes. Insulin stimulated AKT phosphorylation in lung fibroblasts was reduced by αIR3 antibody (data not shown) which suggested that insulin was signaling through IGF-1R. In differentiated adipocytes, we found that insulin stimulated AKT phosphorylation was not sensitive to αIR3. IGF-1 stimulated AKT phosphorylation was equally robust and was sensitive to αIR3. Compound 5 inhibited IGF-1 stimulated AKT phosphorylation in adipocytes with a slightly reduced potency compared to autophosphorylation in the fibroblast system

(IC_{50} = 300 and 42 nM respectively). The selectivity for IGF-1R over IR was similar in both systems.

We conducted crystallization trials in the presence of compound 5 with various forms of IGF-1R and IR to help us better understand the compound binding mode. Acceptable crystals were obtained with non-phosphorylated IR. The inhibitor-bound protein is in an overall inactive conformation. A striking feature is the position of Phe-1151 of the DFG loop. In non-phosphorylated apo-IR, Phe-1151 resides in the adenine binding pocket, partially blocking the ATP site. In the inhibitor-bound structure Phe-1151 is repositioned by ~4 Å to accommodate inhibitor binding. In non-phosphorylated apo-IGF-1R the corresponding Phe, Phe-1124, is in a different position than in non-phosphorylated apo-IR. We did not obtain a non-phosphorylated IGF-1R structure bound to compound 5, but it is possible that the difference in the initial position of Phe-1124 contributes to the selectivity observed. For active IR, Phe-1151 points into the interior of the protein and the C helix is shifted down towards the C-terminal lobe. This conformation would block binding of the compound which probably explains the observed preference for the non-phosphorylated conformation of the receptor.

A variety of ATP-competitive kinase inhibitors of IGF-1R are in pre-clinical or clinical development for the treatment of cancer [37–39]. These molecules can be classified based upon the degree of selectivity for IGF1R compared to IR. For example, GSK4945, BMS-554417, and PQIP appear to be equipotent inhibitors of the two receptors whereas NVP-AEW541 exhibits selectivity for IGF-1R in tissue culture but not in assays with activated purified receptor kinase domains [15–17,19]. Compound 5 is selective in cells like NVP-AEW541. However, the mechanism appears to be different since NVP-AEW541 does not bind preferentially to non-activated IGF-1R. It is unknown how selectivity over IR will ultimately affect the clinical utility of small-molecule IGF-1R inhibitors. Inhibition of IR has been shown to produce expected increases in glucose and insulin [8,37]. In contrast, it is hypothesized that IR or hybrid IGF-1R-IR receptors contribute to tumor growth and survival, so IGF-1R selectivity might result in reduced efficacy in some tumor types [39].

Compound 5 brings an additional dimension into consideration for IGF-1R-targeted therapies, preferential binding to non-activated receptor. The biological properties and structural design of compounds with this binding mode have been recognized and discussed [40,41]. Improved selectivity towards other kinases is a potential advantage of inactive-state binding compounds. Compounds 1 and 5 appear to be very selective based upon the inhibition of purified kinases (Table 2). However, it is possible that the compound selectivity in cells may be different since in vitro assays require the use of activated kinases. Imatinib (Gleevec®) and lapatinib (Tykerb®) are two clinically approved drugs that bind to the inactive-like conformations of BCR-Abl and EGFR/ErbB-2 respectively. These molecules demonstrate additional properties of inactive-state binding. Lapatinib has a very slow off-rate and prolonged duration of effect in tissue culture compared to compounds that bind to the active-like conformation [42]. Imatinib inactive-state binding affects the selectivity compared to compounds that bind the active state [43]. A disadvantage of this binding mode is that mutations in non-essential residues, such as the active-site gatekeeper residue, have been shown to impart resistance to these agents [44,45].

In summary, using a cell-based assay as a primary screen, we have discovered a compound series that preferentially binds to the ATP substrate site of non-activated IGF-1R. This binding-mode presumably contributes to IGF-1R selectivity over IR and other kinases. Our results also highlight an additional advantage; inactive-state binding reduces the negative impact the high-cellular ATP concentration has on inhibitor potency. Exploiting this binding mode may allow for the future discovery of IGF-1R-selective therapies that lack potential side effects associated with inhibition of IR. Further, our results highlight the benefits of using cell-based assays to identify selective inhibitors for kinases with high homology.

References

[1] Yarden Y, Ullrich A. Molecular analysis of signal transduction by growth factors. Biochemistry 1988;27:3113–9.
[2] Favelyukis S, Till JH, Hubbard SR, Miller WT. Structure and autoregulation of the insulin-like growth factor 1 receptor kinase. Nat Struct Mol Biol 2001;8:1058–63.
[3] Blakesley VA, Scrimgeour A, Esposito D, Le Roith D. Signaling via the insulin-like growth factor-I receptor: does it differ from insulin receptor signaling? Cytokine Growth Factor Rev 1996;7:153–9.
[4] Manning BD, Cantley LC. AKT/PKB signaling: navigating downstream. Cell 2007;129:1261–74.
[5] Peruzzi F, Prisco M, Dews M, Salomoni P, Grassilli E, Romano G, et al. Multiple signaling pathways of the insulin-like growth factor 1 receptor in protection from apoptosis. Mol Cell Biol 1999;19:7203–15.
[6] Baserga R, Hongo A, Rubini M, Prisco M, Valentinis B. The IGF-I receptor in cell growth, transformation and apoptosis. Biochim Biophys Acta (BBA)—Rev Cancer 1997;1332:F105–26.
[7] Lopez T, Hanahan D. Elevated levels of IGF-1 receptor convey invasive and metastatic capability in a mouse model of pancreatic islet tumorigenesis. Cancer Cell 2002;1:339–53.
[8] Miller BS, Yee D. Type I insulin-like growth factor receptor as a therapeutic target in cancer. Cancer Res 2005;65:10123–7 [Review] [57 refs].
[9] Yuen JS, Macaulay VM. Targeting the type 1 insulin-like growth factor receptor as a treatment for cancer. Expert Opin Therapeutic Target 2008;12:589–603.
[10] Dancey J, Sausville EA. Issues and progress with protein kinase inhibitors for cancer treatment. Nat Rev Drug Discov 2003;2:296–313.
[11] Fabian MA, Biggs III WH, Treiber DK, Atteridge CE, Azimioara MD, Benedetti MG, et al. A small molecule-kinase interaction map for clinical kinase inhibitors. Nat Biotechnol 2005;23:329–36.
[12] Mukherjee A, Dhadda AS, Shehata M, Chan S. Lapatinib: a tyrosine kinase inhibitor with a clinical role in breast cancer. Expert Opin Pharmacother 2007;8:2189–204.
[13] Wheatley-Price P, Shepherd FA. Epidermal growth factor receptor inhibitors in the treatment of lung cancer: reality and hopes. Curr Opin Oncol 2008;20:162–75.
[14] Bell IM, Stirdivant SM, Ahern J, Culberson JC, Darke PL, Dinsmore CJ, et al. Biochemical and structural characterization of a novel class of inhibitors of the type 1 insulin-like growth factor and insulin receptor kinases. Biochemistry 2005;44:9430–40.
[15] Garcia-Echeverria C, Pearson MA, Marti A, Meyer T, Mestan J, Zimmermann J, et al. In vivo antitumor activity of NVP-AEW541. A novel, potent, and selective inhibitor of the IGF-IR kinase. Cancer Cell 2004;5:231–9.
[16] Haluska P, Carboni JM, Loegering DA, Lee FY, Wittman M, Saulnier MG, et al. In vitro and in vivo antitumor effects of the dual insulin-like growth factor-I/insulin receptor inhibitor, BMS-554417. Cancer Res 2006;66:362–71.
[17] Ji QS, Mulvihill MJ, Rosenfeld-Franklin M, Cooke A, Feng L, Mak G, et al. A novel, potent, and selective insulin-like growth factor-I receptor kinase inhibitor blocks insulin-like growth factor-I receptor signaling in vitro and inhibits insulin-like growth factor-I receptor dependent tumor growth in vivo. Mol Cancer Ther 2007;6:2158–67.
[18] Ullrich A, Gray A, Tam AW, Yang-Feng T, Tsubokawa M, Collins C, et al. Insulin-like growth factor I receptor primary structure: comparison with insulin receptor suggests structural determinants that define functional specificity. EMBO J 1986;5:2503–12.
[19] Emmitte KA, Wilson BJ, Baum EW, Emerson HK, Kuntz KW, Nailor KE, et al. Discovery and optimization of imidazo[1,2-a]pyridine inhibitors of insulin-like growth factor-1 receptor (IGF-1R). Bioorg Med Chem Lett 2009;19:1004–8.
[20] Brignola PS, Lackey K, Kadwell SH, Hoffman C, Horne E, Carter HL, et al. Comparison of the biochemical and kinetic properties of the type 1 receptor tyrosine kinase intracellular domains. Demonstration of differential sensitivity to kinase inhibitors. J Biol Chem 2002;277:1576–85.
[21] McDonald OB, Chen WJ, Ellis B, Hoffman C, Overton L, Rink M, et al. A scintillation proximity assay for the Raf/MEK/ERK kinase cascade: high-throughput screening and identification of selective enzyme inhibitors. Anal Biochem 1999;268:318–29.
[22] Kaleko M, Rutter WJ, Miller AD. Overexpression of the human insulinlike growth factor I receptor promotes ligand-dependent neoplastic transformation. Mol Cell Biol 1990;10:464–73.

[23] Debad JD, Glezer EN, Wohlstadter JN, Sigal GB. Clinical and biological applications of ECL. In: Bard AJ, editor. Electrogenerated chemiluminescence. New York: Marcel Dekker; 2004. p. 43–78.

[24] Baer K, Al-Hasani H, Parvaresch S, Corona T, Rufer A, Nolle V, et al. Dimerization-induced activation of soluble insulin/IGF-1 receptor kinases: an alternative mechanism of activation. Biochemistry 2001;40:14268–7.

[25] Wei L, Hubbard SR, Hendrickson WA, Ellis L. Expression, characterization, and crystallization of the catalytic core of the human insulin receptor protein-tyrosine kinase domain. J Biol Chem 1995;270:8122–30.

[26] Park YW, Cummings RT, Wu L, Zheng S, Cameron PM, Woods A, et al. Homogeneous proximity tyrosine kinase assays: scintillation proximity assay versus homogeneous time-resolved fluorescence. Anal Biochem 1999;269:94–104.

[27] Songyang Z, Kermit L, Eck MJ, Harrison SC, Feldman RA, Mohammadi M, et al. Catalytic specificity of protein-tyrosine kinases is critical for selective signalling. Nature 1995;373:536–9.

[28] Braunwalder AF, Yarwood DR, Sills MA, Lipson KE. Measurement of the protein tyrosine kinase activity of c-src using time-resolved fluorometry of europium chelates. Anal Biochem 1996;238:159–64.

[29] Otwinowski Z, Minor W. Processing of X-ray diffraction data collected in oscillation mode. In: Carter WC, editor. Methods in enzymology macromolecular crystallography part A, vol. 276. Academic Press; 1997. p. 307–26.

[30] Copeland RA. Reversible inhibitors. In: Enzymes: a practical introduction to structure, mechanism and data analysis. New York: John Wiley and Sons; 2000 . p. 266–304.

[31] Li W, Miller WT. Role of the activation loop tyrosines in regulation of the insulin-like growth factor I receptor-tyrosine kinase. J Biol Chem 2006;281:23785–91.

[32] Rohlik QT, Adams D, Kull J, Jacobs S. An antibody to the receptor for insulin-like growth factor I inhibits the growth of MCF-7 cells in tissue culture. Biochem Biophys Res Commun 1987;149:276–81.

[33] Hubbard SR. Crystal structure of the activated insulin receptor tyrosine kinase in complex with peptide substrate and ATP analog. EMBO J 1997;16:5572–81.

[34] Hubbard SR, Wei L, Hendrickson WA. Crystal structure of the tyrosine kinase domain of the human insulin receptor. Nature 1994;372:746–54.

[35] Munshi S, Hall DL, Kornienko M, Darke PL, Kuo LC. Structure of apo, unactivated insulin-like growth factor-1 receptor kinase at 1.5 Å resolution. Acta Crystallogr Section D—Biol Crystallogr 2003;59:1725–30.

[36] Munshi S, Kornienko M, Hall DL, Reid JC, Waxman L, Stirdivant SM, et al. Crystal structure of the Apo, unactivated insulin-like growth factor-1 receptor kinase. Implication for inhibitor specificity. J Biol Chem 2002;277:38797–802.

[37] Gualberto A, Pollak M. Emerging role of insulin-like growth factor receptor inhibitors in oncology: early clinical trial results and future directions. Oncogene 2009.

[38] Lindsay CR, Chan E, Evans TR, Campbell S, Bell P, Stephens AW, et al. Phase I dose escalation study of continuous oral dosing of OSI-906, an insulin like growth factor-1 receptor (IGF-1R) tyrosine kinase inhibitor, in patients with advanced solid tumors. J Clin Oncol (Meeting Abstracts) 2009;27:2559.

[39] Rodon J, DeSantos V, Ferry RJ, Kurzrock R. Early drug development of inhibitors of the insulin-like growth factor-I receptor pathway: lessons from the first clinical trials. Mol Cancer Ther 2008;7:2575–88.

[40] Backes AC, Zech B, Felber B, Klebl B, Muller G. Small-molecule inhibitors binding to protein kinase. Part II: the novel pharmacophore approach of type II and type III inhibition. Expert Opin Drug Discov 2008;3:1427–49.

[41] Noble MEM, Endicott JA, Johnson LN. Protein kinase inhibitors: insights into drug design from structure. Science 2004;303:1800–5.

[42] Wood ER, Truesdale AT, McDonald OB, Yuan D, Hassell A, Dickerson SH, et al. A unique structure for epidermal growth factor receptor bound to GW572016 (Lapatinib): relationships among protein conformation, inhibitor off-rate, and receptor activity in tumor cells. Cancer Res 2004;64:6652–9.

[43] Vajpai N, Strauss A, Fendrich G, Cowan-Jacob SW, Manley PW, Grzesiek S, et al. Solution conformations and dynamics of ABL kinase-inhibitor complexes determined by NMR substantiate the different binding modes of imatinib/nilotinib and dasatinib. J Biol Chem 2008;283:18292–302.

[44] Gilmer TM, Cable L, Alligood K, Rusnak D, Spehar G, Gallagher KT, et al. Impact of common epidermal growth factor receptor and HER2 variants on receptor activity and inhibition by lapatinib. Cancer Res 2008;68:571–9.

[45] Gora-Tybor J, Robak T. Targeted drugs in chronic myeloid leukemia. Curr Med Chem 2008;15:3036–51.

[46] Gaudet EA, Huang KS, Zhang Y, Huang W, Mark D, Sportsman JR. A homogeneous fluorescence polarization assay adaptable for a range of protein serine/threonine and tyrosine kinases. J Biomol Screen 2003;8:164–75.

[47] Angell RM, Atkinson FL, Brown MJ, Chuang TT, Christopher JA, Cichy-Knight M, et al. N-(3-Cyano-4,5,6,7-tetrahydro-1-benzothien-2-yl)amides as potent, selective, inhibitors of JNK2 and JNK3. Bioorg Med Chem Lett 2007;17: 1296–301.